

Optimization of a Low Reynolds Number Airfoil with Flexible Membrane

Ori Levin and Wei Shyy¹

Abstract: Typical low Reynolds number airfoils suffer from reduced lift-to-drag ratio and are prone to flow separation. In order to improve the aerodynamic performance of such airfoils in an unsteady freestream, the concept of passive control is investigated. In this study, a membrane with varying thickness distribution and mechanical properties is attached on the upper surface of a modified Clark-Y airfoil and is free to move upwards and downwards in response to the pressure difference across it. The response surface method is employed to investigate the individual and collective effects of the membrane's prestress, elastic modulus, and thickness distribution on aerodynamic characteristics, as well as to optimize the performance of the airfoil. It is demonstrated that the aerodynamic performance of the airfoil can be improved with such a passive control approach based on the optimized design variables.

1 Introduction

Micro air vehicles (μ AVs) have recently received substantial interests for a variety of possible applications [Shyy, Berg and Ljunqvist (1999)]. Currently, such air vehicles have a target length under 15 cm, a flight speed of 15 m/s, and a range of at least several kilometers. This means that the Reynolds number is around 10^4 - 10^5 . At this flight speed and Reynolds number, the aerodynamic performance of the airfoil is very sensitive to fluctuations in wind speed, which is not necessarily small compared to the flight speed. Since the flow surrounding the leading edge is usually laminar, the fluid momentum is often not strong enough to overcome the adverse pressure gradient on the aft side of the airfoil to prevent laminar separation from occurring. Once separated, the boundary layer disturbance amplification rates greatly increase, inducing transition toward turbulence. The position of the

transition region and the structure of the separated bubble are sensitive to the Reynolds number. Consequently, it is difficult to construct conventional rigid airfoils with good aerodynamic performance in such unsteady, low Reynolds number flights.

From observation of bird and bat flights, as well as man-made sails, it appears that flexible wings would be desirable for sustained flight. An extensive summary and reference collection of models and observations concerning animal flights relevant to μ AVs can be found in Shyy, Berg and Ljunqvist (1999). Boundary layer control also appears to have a positive effect on the performance. There are two different types of boundary layer control. Passive methods like flaps, slats, slots, fences or vortex generators and active methods like suction or blowing. Both methods either add high energy fluid or remove low energy fluid in a region on the suction side of the wing where the boundary layer tends to separate. A flexible wing that passively changes its shape due to the surrounding flow to improve the performance is an interesting alternative [Shyy, Berg and Ljunqvist (1999), Shyy, Jenkins and Smith (1997), Shyy, Klevebring, Nilsson, Sloan, Carroll and Fuentes (1999), Shyy and Smith (1997)].

One way to express an airfoil's aerodynamic performance is through the lift-to-drag ratio C_l/C_d , which is a function of both the angle of attack and the freestream Reynolds number. C_l and C_d are here the *lift* and *drag coefficients*, respectively. Another way is in terms of the *flight power requirement for steady flight*

$$P = W \frac{C_d}{C_l^{3/2}} \sqrt{\frac{2W}{\rho S}} \quad (1)$$

where ρ is the *fluid density*, W and S are the aircraft's *weight* and *projected wing area*, respectively. The coefficients for a given profile are functions of both the angle of attack and the freestream Reynolds number. The *power index* defined as

¹ Department of Aerospace Engineering,
Mechanics and Engineering Science
University of Florida
Gainesville, FL 32611, U.S.A.

$$PI = C_l^{3/2} / C_d \quad (2)$$

is used here to measure the performance. The *average power index* PI_{avg} , which is the integral of the power index over time divided by the time period in one unsteady cycle, is used to measure the overall performance in one cycle.

In the present study we investigate the performance of a semi-flexible airfoil in an unsteady, low Reynolds number environment. A flexible, massless membrane with varying thickness distribution and mechanical properties is attached on the upper surface of a modified Clark-Y airfoil and is free to move upwards and downwards in response to the pressure difference across it. The response surface method is employed to investigate the individual and collective effects of the membrane's prestress, elastic modulus, and thickness distribution on aerodynamic characteristics, as well as to optimize the average power index.

2 Membrane Formulation

2.1 Flexible wings

In the following, we first present a summary of flexible membrane that serves as a basis for this work. A massless membrane with zero thickness attached at the leading and trailing edges is illustrated in Fig. 1. The membrane is subject to both *fluid dynamic pressure* p and net *shear stress* τ according to the force balance in normal and tangential directions

$$\frac{d^2y}{dx^2} \left(1 + \frac{dy}{dx} \right)^{-3/2} = -\frac{\Delta p}{T}, \quad \frac{dT}{d\xi} = -\Delta\tau \quad (3)$$

where T is the *membrane tension*. The differences in pressure and shear stress are defined as the values at the lower side minus the values at the upper side. More details about the *elastic boundary value problem*, Eq. (3), can be found in Shyy, Udaykumar, Rao and Smith (1996). A recent article by Rugonyi and Bathe (2001) investigates the issues related to fluid flow and structure interactions from a finite element perspective.

Previous studies indicate that by letting the lifting surface move and deform, more favorable aerodynamic performance can be achieved, in a fluctuating low Reynolds

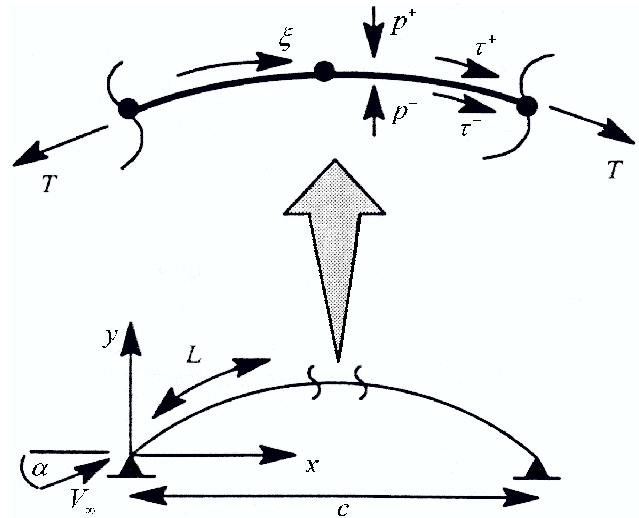


Figure 1 : End constrained elastic membrane.

number environment. In a directly related work, Shyy, Klevebring, Nilsson, Sloan, Carroll and Fuentes (1999) have investigated the potential of a flexible airfoil by allowing a portion of the upper surface of the Clark-Y airfoil to be exchanged by a massless membrane. The membrane can instantaneously adjust its shape according to the force balance normal to the membrane. In that work, the elastic modulus and membrane thickness are constant along the membrane. The XFOIL [Drela (1989)] code, which will be described in detail, was modified to handle a semi-flexible airfoil in an unsteady environment. The freestream Reynolds number was sinusoidal with 30% oscillations about its mean value of 8×10^4 . Fig. 2 shows a sequence of the shapes of the semi-flexible airfoil compared with the original rigid Clark-Y airfoil.

It can be seen in Fig.3 that the overall performance is slightly better for the semi-flexible airfoil mainly depending on the substantial dip for the rigid airfoil's performance at the lower Reynolds numbers. That dip is most severe for the case with zero angle of attack.

The maximum lift coefficient of the semi-flexible airfoil is no better than that of the rigid airfoil. However, the semi-flexible airfoil is less sensitive to fluctuations in Reynolds number and maintains a higher lift coefficient during the slower freestream velocity. Qualitatively, the thickness of the semi-flexible airfoil increases as the flight speed increases and decreases as the flight speed decreases. This trend is consistent with the general ex-

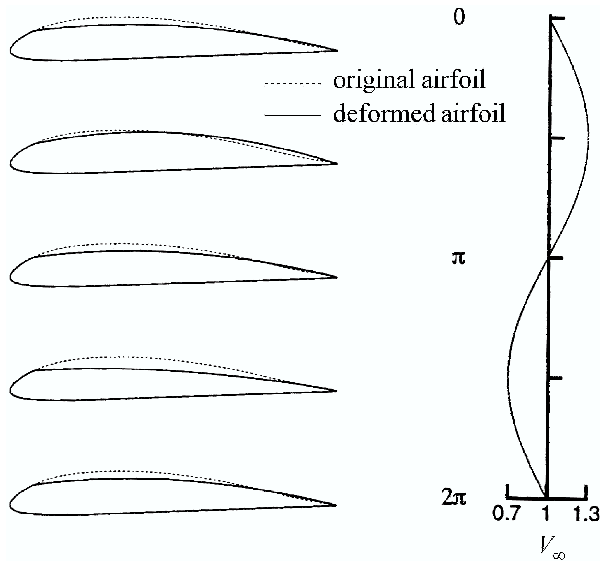


Figure 2 : Membrane deformations during a full period oscillation about $Re=8.0 \times 10^4$.

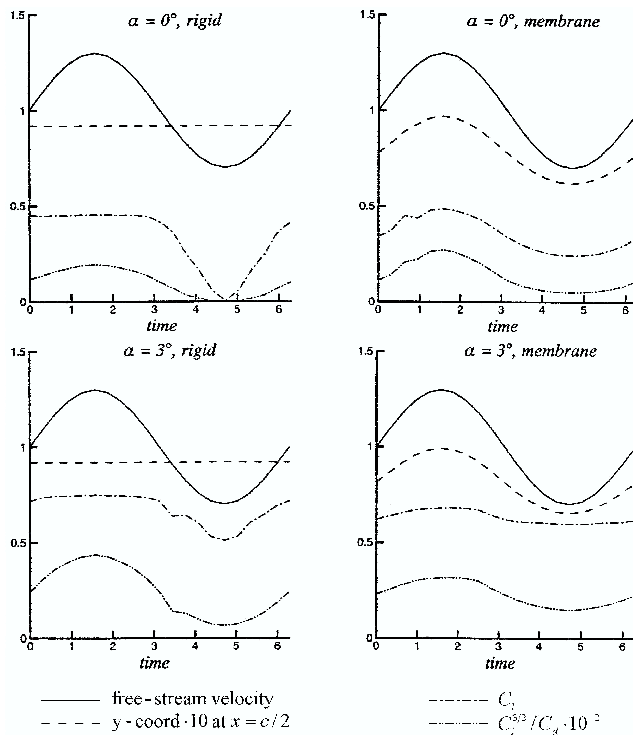


Figure 3 : Comparison between rigid and membrane modified Clark-Y airfoils during a full period oscillation about $Re=8.0 \times 10^4$.

pectation that a thinner airfoil performs better in a low Reynolds number environment.

2.2 Governing equations

In the following, the formulation for membrane dynamics will be presented by accounting for three parameters: prestress, elastic modulus, and thickness distribution. Consider a rigid airfoil where a part of the upper side is replaced with a massless membrane, which is free to move both upwards and downwards. The *membranes initial length* L_0 is defined to be the straight line between the two attached endpoints. That is the case when the airfoil is still and the pressure difference Δp between the upper side and the inside of the airfoil is zero. As soon as the pressure difference changes, such as in flight, the membrane will instantaneously deform according to the *membrane equilibrium equation*

$$\kappa = -\frac{\Delta p}{T} \quad (4)$$

where κ describes the *membrane curvature* and the membrane tension T (force per meter span) is defined as

$$T = ({}^0S + E\delta) \cdot h \quad (5)$$

The prestress 0S is also defined as the stress in the membrane when the airfoil is still and hence the membrane describes a straight line. The elastic modulus E is a material constant that is supposed to be constant along the membrane. The *membrane strain* δ is a dimensionless parameter defined as

$$\delta = \frac{L - L_0}{L_0} \quad (6)$$

where L is the *membrane length*. The pressure difference is defined as the difference between the outside and the inside of the airfoil

$$\Delta p = p_{\text{out}} - p_{\text{in}} \quad (7)$$

The pressure inside the airfoil is set to the stagnation pressure and is varying with the freestream and since the

velocity inside the airfoil therefore is zero, the Bernoulli equation gives

$$p_{in} = p_{\infty} + q_{\infty} \quad (8)$$

Equation (7) together with the definition of the pressure coefficient gives

$$\Delta p = q_{\infty} C_p + p_{\infty} - p_{in} \quad (9)$$

and the special case that the inside pressure is equal to the stagnation pressure implies that

$$\Delta p = q_{\infty} (C_p - 1) \quad (10)$$

The membrane formulation can be written in the dimensionless form if appropriate dimensionless parameters are introduced. The following normalization is used where ${}^0q_{\infty}$ is the *dynamic pressure* at time zero.

$$\bar{T} = \frac{T}{{}^0Sh} \quad (11)$$

$$\bar{E} = \frac{E}{{}^0S} \quad (12)$$

$$\bar{q}_{\infty} = \frac{q_{\infty}}{{}^0q_{\infty}}, \quad \bar{p} = \frac{p}{{}^0q_{\infty}} \quad (13)$$

$$\bar{\kappa} = \kappa \cdot c \quad (14)$$

$$\bar{x} = \frac{x}{c}, \quad \bar{y} = \frac{y}{c}, \quad \bar{s} = \frac{s}{c} \quad (15)$$

If the normalized parameters, defined in Eqs (11) through (14), are substituted into Eqs (4), (5) and (9) we obtain the dimensionless relations

$$\bar{\kappa} = -\frac{\bar{\Delta p}}{\Pi_2 \cdot \bar{T}} \quad (16)$$

$$\bar{T} = 1 + \bar{E}\delta \quad (17)$$

$$\bar{\Delta p} = \bar{q}_{\infty} C_p + \bar{p}_{\infty} - \bar{p}_{in} \quad (18)$$

where Π_2 is a *dimensionless group* defined as

$$\Pi_2 = \frac{{}^0Sh}{{}^0q_{\infty}c} \quad (19)$$

Shyy, Klevebring, Nilsson, Sloan, Carroll and Fuentes (1999) used in their formulation another variant of the *non-dimensional membrane equilibrium equation*

$$\bar{\kappa} = -\frac{\bar{\Delta p}}{\Pi_1^3 \bar{T}} \quad (20)$$

where the *non-dimensional elastic number* Π_1 is given by

$$\Pi_1 = \left(\frac{Eh}{{}^0q_{\infty}c} \right)^{\frac{1}{3}} \quad (21)$$

The aeroelastic response of a membrane is controlled exclusively by Π_1 in the limit of vanishing prestress and exclusively by Π_2 in the limit of vanishing material stiffness. The membrane equilibrium equations, Eqs (16) and (20), are non-dimensional versions of the normal force balance in the elastic boundary value problem, Eq. (3).

2.3 Variable thickness membrane

The parameters that are selected to control the shape of the membrane are (i) the prestress 0S , (ii) the elastic modulus E , and (iii) the membrane thickness h . The pressure difference and the membrane strain is determined by the flow and the shape. Shyy, Klevebring, Nilsson, Sloan, Carroll and Fuentes (1999) used in their simulations a constant membrane thickness and therefore also a constant prestress along their membrane. Their results show that the curvature variation was quite small. In fact the only parameter that affects the curvature for a membrane with constant thickness distribution is the pressure difference. However, a membrane with variable thickness can easily be formed within certain limits. But a variable thickness also implies a variable prestress since

$${}^0S = \frac{{}^0T}{h} \quad (22)$$

where 0T is the *initial membrane tension* when $\delta=0$. That tension will of course be constant along the membrane so the product 0Sh will be a constant implying that the dimensionless group, Eq. (19), also will be a constant. Thus the only parameter where the thickness distribution comes into account in Eqs. (16) through (19) is

the normalized elastic modulus \bar{E} . To make it possible to use a constant reference value of the prestress as in-data a corresponding reference thickness is introduced such as

$${}^0T = {}^0S_{\text{ref}}h_{\text{ref}} \quad (23)$$

Then the prestress distribution is given by Eq. (22). The membrane thickness is allowed to vary between a minimum thickness h_{min} and a maximum thickness h_{max} .

2.4 Constant lift formulation

In a real situation a flying vehicle would require a constant lift to maintain level flying. The lift coefficient is defined as

$$C_l = \frac{F}{q_{\infty}c} \quad (24)$$

where F denotes lift per meter span. Consequently, to keep the lift constant in a variable freestream the lift coefficient has to be inversely proportional to the dynamic pressure. To fulfil that, the angle of attack has to vary. If nothing is done the air vehicle will receive a vertical acceleration according to the force balance

$$m\ddot{y} = F - mg \quad (25)$$

In that way the angle of attack will automatically adjust itself. It will increase when the air vehicle starts to fall in a decreasing freestream and decrease when the air vehicle picks up altitude in an increasing freestream. By integration in time of Eq. (25) the vertical freestream component can be received as

$$v_y = -\dot{y} = gt - \int \frac{F}{m} dt \quad (26)$$

The minus sign is there because the freestream velocity is opposite to the air vehicle velocity. Consider Fig. 4. The angle between the freestream direction and the horizontal line is given by

$$\beta = \arctan(v_y/v_x) \quad (27)$$

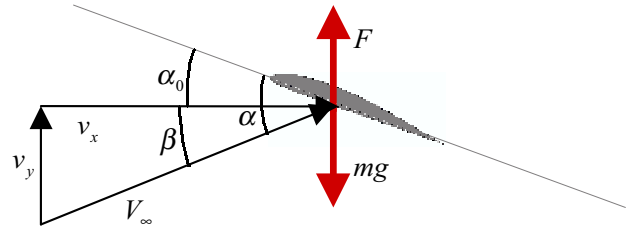


Figure 4 : Relative angle of attack on airfoil with vertical moments caused by freestream fluctuations.

The new relative angle of attack is then given by

$$\alpha = \alpha_0 + \beta \quad (28)$$

The freestream velocity, which will not be horizontal when the air vehicle is falling or gaining altitude, and the Reynolds number will of course be affected by the vertical movements.

3 Computational Methodology

To facilitate the present study we have employed XFOIL [Drela (1989)] which models inviscid or coupled inviscid/boundary-layer flows around rigid airfoils in steady, subsonic flow, as the starting point for software development. XFOIL uses a two-equation boundary layer integral formulation based on dissipation closure for both laminar and turbulent flow [Drela and Giles (1987)]. It includes in the laminar formulation a transition prediction formulation based on the spatial amplification theory. A linear model is employed to predict transition, which accounts for the growth of the amplitude \bar{n} of the most amplified Tollmien-Schlichting wave. In the turbulent formulation it also includes a lag equation to account for lags in the response of the turbulent stresses to changing flow conditions. The inviscid freestream is computed using a linear-vorticity panel method. The boundary layer and transition equations are solved simultaneously with the inviscid flowfield by a global Newton method.

3.1 Inviscid formulation

The airfoil contour and wake trajectory are discretized into flat panels, with N panel nodes on the airfoil, and N_w nodes on the wake as shown in Fig. 5.

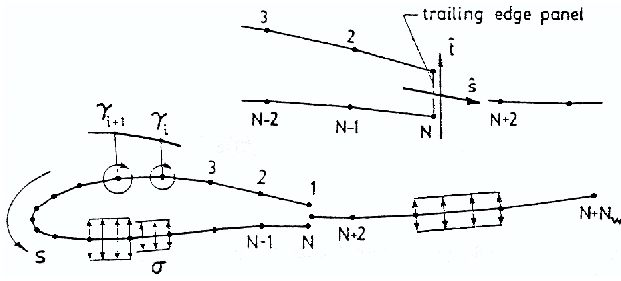


Figure 5 : Airfoil and wake paneling with vorticity and source distributions, with trailing edge detail.

A linear *vorticity distribution* is associated with each airfoil panel. Each airfoil and wake panel also has a constant *source strength* related to viscous layer quantities. The streamfunction is given by

$$\Psi(x, y) = u_{\infty}y - v_{\infty}x + \frac{1}{2\pi} \int \gamma(s) \ln r(s; x, y) ds + \frac{1}{2\pi} \int \sigma(s) \vartheta(s; x, y) ds \quad (29)$$

where s is the coordinate along the airfoil surface, r is the magnitude of the vector from the surface point at s and the field point (x, y) , ϑ the angle of the vector, and u_{∞} and v_{∞} are the x and y -components of the undisturbed freestream velocity. If the airfoil trailing edge has a finite thickness a panel of uniform source strength and vortex strength must be placed across the gap. By defining unit streamfunctions for each panel in terms of local panel coordinates and requiring that the streamfunction is equal to some constant value Ψ_0 on the airfoil surface, the following linear system, which can be further examined in Drela (1989) results in

$$\sum_{j=1}^N a_{ij} \gamma_j - \Psi_0 = -u_{\infty}y_i + v_{\infty}x_i - \sum_{j=1}^{N+N_w-1} b_{ij} \sigma_j \quad (30)$$

The coefficient matrices a_{ij} and b_{ij} are fully determined from the above mentioned unit streamfunctions. Combining the linear system, Eq. (30), with a Kutta condition for the trailing edge

$$\gamma_1 + \gamma_N = 0 \quad (31)$$

gives a linear system for the N node values γ_i and the airfoil surface streamfunction Ψ_0 . A special treatment is required for an airfoil with a sharp trailing edge. The $i=1$ equation and the $i=N$ equation in Eq. (30) are then identical and the linear system is singular. To circumvent this problem, the $i=N$ equation is replaced by an extrapolation of the mean vortex strength between the top and bottom of the trailing edge

$$(\gamma_3 - 2\gamma_2 + \gamma_1) - (\gamma_{N-2} - 2\gamma_{N-1} + \gamma_N) = 0 \quad (32)$$

Since the flow inside the airfoil is stagnant, the velocity distribution is determined by the vorticity distribution on the airfoil surface as

$$u_{ei} = \pm \gamma_i \quad (33)$$

where u_e is the total fluid velocity on the airfoil surface. The *inviscid surface velocity*, u_e , is assumed equal to the *boundary layer edge velocity* of the viscous formulation.

3.2 Viscous formulation

The viscous formulation is essentially the same as the transonic ISES code described in Drela and Giles (1987). Some changes have been incorporated to improve the prediction of the ‘base drag’ from blunt trailing edges. The streamline along the boundary layer edge, where the velocity is u_e , is displaced normal to the wall by a distance equal to the local *displacement thickness* δ^* . The present formulation employs the following standard *integral momentum* and *kinetic energy shape parameter* equations based on the streamwise coordinate ξ

$$\frac{d\theta^*}{d\xi} + (2 + H - M_e^2) \frac{\theta^*}{u_e} \frac{du_e}{d\xi} = \frac{C_f}{2} \quad (34)$$

$$\theta^* \frac{dH^*}{d\xi} + [2H^{**} + H^*(1 - H)] \frac{\theta^*}{u_e} \frac{du_e}{d\xi} = 2C_D - H^* \frac{C_f}{2} \quad (35)$$

Here $H = \delta^*/\theta$ is the *shape parameter*, $H^* = \theta^*/\theta$ the *kinetic energy shape parameter* and θ is the *momentum layer thickness*. Also a *kinetic energy layer thickness*

θ^* is defined along with a maximum *shear layer coefficient* C_τ that represents a measure of the shear stresses in the wake. A *shear stress lag equation*, which has been slightly modified from the original formulation [Drela and Giles (1987)] to improve the lift and drag prediction near stall, is used in turbulent flow regions

$$\frac{\delta}{C_\tau} \frac{dC_\tau}{d\xi} = 5.6 \left(C_{\tau_{EQ}}^{0.5} - C_\tau^{0.5} \right) + 2\delta \left\{ \frac{4}{3\delta^*} \left[\frac{C_f}{2} - \left(\frac{H_k - 1}{6.7H_k} \right)^2 \right] - \frac{1}{u_e} \frac{du_e}{d\xi} \right\} \quad (36)$$

For the laminar regions, Eq. (36) is replaced by a *rate equation* that models the growth of the amplitude \tilde{n} of the most amplified Tollmien-Schlichting wave

$$\frac{d\tilde{n}}{d\xi} = \frac{d\tilde{n}}{dRe_\theta} (H_k) \frac{dRe_\theta}{d\xi} (H_k, \theta^*) \quad (37)$$

where the Reynolds number Re_θ is based on the momentum layer thickness. The empirical relation $d\tilde{n}/Re_\theta$ is a correlation of spatial growth rates computed from solutions to the Orr-Sommerfeld equation and $Re_\theta/d\xi$ is obtained from the properties of the Falkner-Skan profile family. The transition point is defined by the location where \tilde{n} reaches a user-specified critical value \tilde{n}_{crit} . This parameter is in practice used to represent the background disturbance level and has a dramatic effect on low Reynolds number airfoil performance. The governing equations, Eqs. (34) to (37), are discretized using two-point central differences. The boundary layer variables θ , δ^* , C_τ or \tilde{n} and u_e are defined to be located at the panel nodes. In laminar regions, \tilde{n} replaces C_τ . Each panel therefore has three coupled nonlinear equations associated with it.

The influence of the viscous layer on the potential flow is modeled by the wall transpiration concept if the local source strength σ is equal to the local gradient of *mass defect*, $\mu \equiv u_e \delta^*$

$$\sigma_i = \frac{d\mu}{d\xi} = \pm \frac{\mu_{i+1} - \mu_i}{s_{i+1} - s_i} \quad (38)$$

This source distribution is then used together with the linear system, Eq. (30), to calculate u_e in the wake

$$u_{e_i} = \nabla \Psi \cdot \hat{n} = u_\infty \hat{n}_x - v_\infty \hat{n}_y + \sum_{j=1}^N c_{ij}^\gamma \gamma_j + \sum_{j=1}^{N+N_w-1} c_{ij}^\sigma \sigma_j \quad (39)$$

which then is used to solve for the three unknown variables δ , θ , and C_τ in the three Eqs. (34), (35) and (36) or (37). The resulting value of δ gives a new source distribution, Eq. (38), for the inviscid calculation where the new boundary layer edge velocity distribution, Eqs. (33) and (39), is obtained.

3.3 Computational setup for the membrane

XFOIL [Drela (1989)] has been further developed to account for the moving boundary problems. In the modified code, time dependency is introduced to simulate an unsteady flow with an oscillating freestream with the Reynolds number given by

$$Re = Re_{ref} (A \cdot \sin(\omega t) + 1) \quad (40)$$

but in every time step k the solution is based on steady assumptions. A part of the rigid airfoil can be exchanged for a membrane with defined prestress, elastic modulus and thickness distribution. The membrane is panelized in the same way as the rest of the airfoil and divided into a certain number of nodes i . In each time step the membrane is iterated according to Eqs. (16) through (22) with the previous calculated pressure distribution as a starting guess. In the first time step the pressure distribution is calculated for the rigid airfoil. The *surface slope angles*, φ_i and φ_{i+1} , shown in Fig. 6, are determined from the curvature as

$$\frac{d\varphi}{ds} = \kappa \quad (41)$$

which after integration becomes

$$\varphi_{i+1} = \varphi_i + \kappa_i \Delta s \quad (42)$$

where the curvature κ is assumed to be constant between two adjacent nodes. Taking an initial guess for the starting angle φ_1 , the shooting method is used to iterate the

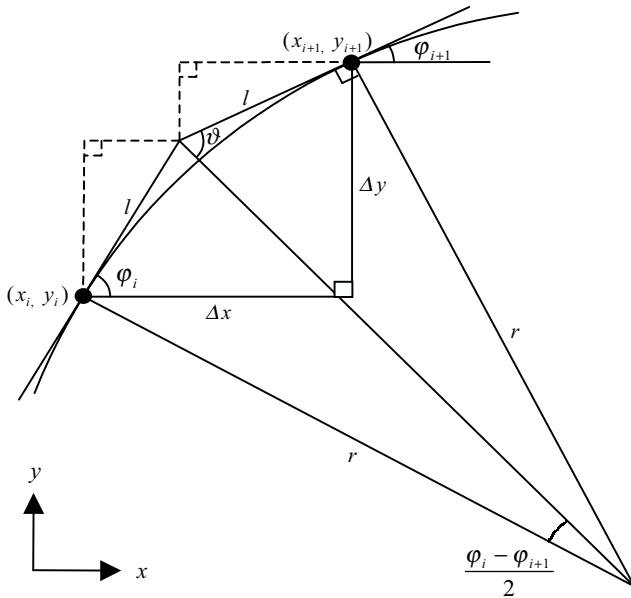


Figure 6 : Membrane coordinate calculation.

membrane coordinates using the angles and curvatures shown in Fig. 6.

The last node on the membrane will probably not match the attach-point with the rigid part of the airfoil. The procedure converges when the difference between the two point's y-coordinates is less than a certain value ϵ_y (a small correction for the x-coordinate is then made). If the membrane's y-coordinate is too high or too low, a new guess for the starting angle is calculated according to

$$\varphi_1^{j+1} = \frac{\varphi_1 + \varphi_{\min}}{2} \text{ or } \varphi_1^{j+1} = \frac{\varphi_1 + \varphi_{\max}}{2} \quad (43)$$

A new δ is calculated through a relaxation method

$$\delta_{j+1} = \delta_j + w(\delta^x - \delta_j) \quad (44)$$

where δ^x is calculated with Eq. (6) and the *relaxation parameter* w is chosen as 0.5. The membrane is recalculated until the δ -change between two calculations is less than a certain value ϵ_δ . The pressure coefficient distribution is calculated through the relaxation method

$$C_p^{j+1} = C_p^j + w(C_p^x - C_p^j) \quad (45)$$

where C_p^x is calculated of the original part of the program and the relaxation parameter w is again chosen as 0.5 (In the first loop the quantities denoted by cross is used instead of the relaxation). A new pressure distribution is then calculated, and another membrane shape is determined corresponding to the new pressure difference. The entire procedure is repeated to obtain a new equilibrium shape corresponding to the new boundary conditions. An equilibrium shape is reached when the coordinatechange in two successive profiles defined by

$$\sum_i \sqrt{(x_i^j - x_i^{j-1})^2 + (y_i^j - y_i^{j-1})^2} \quad (46)$$

is smaller than a certain value ϵ .

4 Results and Discussions

In the following, we present results produced by investigating the individual and collective effects of membrane prestress, elastic modulus, and thickness distribution on the airfoil performance. Then, a response surface technique will be employed to facilitate design optimization of the membrane. The Clark-Y airfoil is selected for illustration. The same conceptual framework can be extended to investigate other suitable low Reynolds number airfoils.

(i) Simulations

Before we can do the simulations for a semi-flexible airfoil with a massless membrane attached at the upper side we have to choose which rigid base shape we should use. This aspect is addressed first.

4.1 Rigid airfoil in unsteady flows

In the present study, in order to see how the aerodynamic performance depends of the thickness in an unsteady environment a number of simulations are done around $Re=8.0 \times 10^4$ and different angles of attack. The freestream Reynolds number is fluctuating 30% about its mean according to Eq. (40).

The investigations are summarized in Table 1 based on the various modifications made to the original Clark-Y airfoil. The thickness of the Clark-Y airfoil is changed by multiplying all the airfoil y coordinates by a *thickness ratio* tr , which is defined as the modified airfoil's thickness divided by the original airfoil's thickness. By doing that

tr	PI_{avg}	C_l at $k=5$	C_l at $k=15$	PI at $k=5$	PI at $k=15$
0.6	7.05	0.27	0.09	15.4	1.11
0.7	7.10	0.30	0.06	12.5	0.58
0.8	8.95	0.36	0.03	19.1	0.19
0.9	9.85	0.40	0.00	21.5	0.00

 $\alpha = 3^\circ$

tr	PI_{avg}	C_l at $k=5$	C_l at $k=15$	PI at $k=5$	PI at $k=15$
0.5	20.1	0.50	0.33	25.9	7.14
0.6	25.4	0.57	0.3	44.1	5.26
0.7	25.0	0.62	0.27	45.8	3.75
0.8	25.6	0.66	0.23	48.3	2.62
0.9	25.9	0.71	0.23	50.5	2.18
1.0	25.6	0.75	0.16	52.2	1.15
1.1	25.4	0.79	0.12	53.5	0.67

 $\alpha = 5^\circ$

tr	PI_{avg}	C_l at $k=5$	C_l at $k=15$	PI at $k=5$	PI at $k=15$
0.6	34.9	0.75	0.67	45.4	10.9
0.7	36.9	0.81	0.64	60.5	9.08
0.8	37.0	0.86	0.62	63.0	7.58
0.9	36.7	0.9	0.59	64.9	6.16
1.0	36.0	0.94	0.51	65.9	4.33

 $\alpha = 0^\circ$

Table 1 : Modified Clark-Y airfoils in a fluctuating freestream around $Re=8.0 \times 10^4$.

the camber will also change in the same rate. It is clear that the fluctuations in power index and lift coefficient increase rapidly with increasing thickness ratio while the average power index does not change very much.

A good airfoil in unsteady conditions should have high power index and lift coefficient that not vary too much and a high average power index. All the results show that the thinner airfoils maintain their performance during the lower Reynolds number while the thicker airfoils have a better performance during the higher Reynolds numbers.

4.2 Flexible airfoil in unsteady flows

The Clark-Y airfoil with a thickness ratio 0.8 is chosen as a base for the membrane. The membrane is attached on the upper side between the dots from approximately $0.1c$ to the trailing edge according to Fig. 7.

The question is how to choose the constants E and ${}^0S_{ref}$ and the function h to optimize the aerodynamic properties of the semi-flexible airfoil. We have chosen approximately the same initial thickness of the rigid and the semi-flexible airfoil to be able to do meaningful comparisons between the both airfoils. In this study this is fulfilled through using the highest point on the upper side of the rigid airfoil as a reference point. The condition on the membrane is that it has to go through that point at time

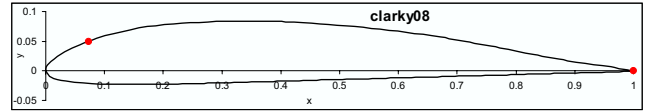


Figure 7 : Modified Clark-Y airfoil with thickness 0.8 of the original Clark-Y. The membrane in the flexible version is attached at the upper side at the dots.

zero.

A number of simulations are performed where the methodology is to produce a sufficient number of design points for the response surface method. The thickness function is chosen from the power law

$$h = As^z + B \quad (47)$$

with the constants A and B chosen to make the minimum and maximum thickness set to prescribed values. In the choice of the thickness distribution function we consider the curvature difference between the forward part and the aft part of the upper side of the airfoil. The curvature should be larger at the forward part and thus the membrane should be thinner there as the case in the power law, Eq. (47). The power z was varied between 0.3 and 7, which was found to yield generally sensible aerodynamic performance. In order to produce a good fit of the response surface in the later described optimization of the membrane quantities, many additional simulations are performed. In total 250 design points were produced. The simulations show that the membrane shape look more like a circle arc for higher prestress, hence, the curvature variation is less. Another way to see it is that the maximum membrane y -value moves backwards towards the center of the airfoil for increasing prestress. For a good airfoil the maximum y -value should be at approximately $1/3$ from the leading edge. The elastic modulus affects the deflection of the membrane. As higher the elastic modulus is, the stiffer the membrane becomes, and the less the deflection is.

4.3 Physical parameters and convergence criteria

The simulations are meant to be based on a Micro Air Vehicle with an airfoil chord of $c=12\text{cm}$ flying in air with pressure 10^5Pa . The velocity fluctuation is along the horizontal (freestream) direction, and of 30% in magnitude

compared to the mean velocity, which is 10m/s corresponding to Reynolds number 8.0×10^4 . The time period during one cycle is three seconds and is divided in 20 time intervals, although the time period and number of time steps are insignificant as long as the membrane is massless and the flow properties are solved independently as a steady case in every time step. The membrane reference thickness is set to $h_{ref}=0.001c$ while the minimum and maximum allowed thickness is $h_{min}=0.1h_{ref}$ and $h_{max}=10h_{ref}$, respectively. Normal values for the elastic modulus in the membrane material, which is supposed to be some kind of gum, are according to material handbooks $0.5\text{-}20\text{MN/m}^2$.

In the original code that deals with steady, rigid calculations the convergence criteria are set to the default values and 140 panels are used for the penalization of the airfoil. The membrane is attached to the nodes 1 and 65, thus the trailing edge and just behind the leading edge on the upper surface, see Fig. 7. The convergence criteria's in the membrane part is set to $\epsilon=5.0 \times 10^{-3}$, $\epsilon_y=1.0 \times 10^{-4}$ and $\epsilon_\delta=5.0 \times 10^{-5}$.

(ii) Optimization

The next task is to find the optimal membrane quantities in order to maximize the average power index as a measurement of the performance.

4.4 Response surface method (RSM)

The approach of RSM [Myers and Montgomery (1995)] is to construct a response surface $\hat{S}(x_j)$ from a series of measured quantities x_j of experiments or numerical analysis. The response surface is a global approximation over the entire design space unlike gradient-based methods, which are sets of local approximations. A standard optimization algorithm is then used to interrogate the response surface for an optimum design. For more detailed discussions of applying this technique for fluid dynamics applications, see Shyy, Papila, Vaidyanathan and Tucker (2001). We also note that a recent paper by Okumura and Kawahara (2000) is of interest also.

In the case of the semi-flexible, modified Clark-Y airfoil, see Fig. 7, the parameters that are allowed to vary to optimize the performance are the prestress ${}^0S_{ref}$, the elastic modulus E and the power z to the power law, Eq. (47). The average power index PI_{avg} is used here as a measurement of the performance. To improve numerical stability the design space is normalized to scale the variables be-

tween zero and one.

$$\begin{aligned} d_1 &= \frac{z - z_{min}}{z_{max} - z_{min}}, & d_2 &= \frac{{}^0S_{ref} - {}^0S_{min}}{{}^0S_{max} - {}^0S_{min}}, \\ d_3 &= \frac{E - E_{min}}{E_{max} - E_{min}} \end{aligned} \quad (48)$$

where the boundaries are

$$\begin{aligned} z_{min} &= 0.3, & z_{max} &= 7.0 \\ {}^0S_{min} &= 1.0\text{N/m}^2, & {}^0S_{max} &= 80\text{kN/m}^2 \\ E_{min} &= 1.25\text{MN/m}^2, & E_{max} &= 19.8\text{MN/m}^2 \end{aligned} \quad (49)$$

A response surface is fit to the 250 simulations by standard least square regression with a polynomial using JMP [SAS Institute Inc. (1995)] a statistical analysis software. Four different orders of polynomial are used and compared with each other and XFOIL. Either a forward or a backward elimination procedure is conducted to eliminate terms and improve the prediction accuracy. The elimination is based on t-statistics [Myers and Montgomery (1995)] which is a measurement of the significance of any individual regression coefficient. The t-statistic of a particular coefficient is given by the value of the coefficient divided by the standard error of the coefficient.

4.5 Forward & backward elimination

The forward elimination begins with the assumption that there are no other regressors in the model than the intercept. An effort is made to find an optimal subset by inserting the regressors one at the time and fit the new model in each step. In each step the regressor with the highest simple correlation with the response is entered in the model. This is also the regressor that will produce the highest t-statistic value. The procedure is terminated if the highest t-statistic value becomes lower than a preselected value.

The backward elimination begins with a model that includes all the candidate regressors. In each step the regressor with the smallest t-statistic value is removed from the model and the new model is fitted. The procedure is terminated if the smallest t-statistic value becomes higher than a preselected value.

4.6 Estimating the accuracy of the response surface

A response surface where terms have been excluded need not necessarily be better than the full model. To compare the different models and estimate the accuracy the adjusted root mean square (RMS) error is used, which is defined as

$$\sigma_a = \sqrt{\sum_{j=1}^n \frac{e_j^2}{n - n_S}} \quad (50)$$

Here e is the error, n the number of design points and n_S the number of coefficients. A lower value of adjusted RMS error indicates a better fit of the response surface in the design points. The variation of the data from its average \bar{S} is denoted as SS_S and is given by

$$SS_S = \sum_{j=1}^n (S_j - \bar{S})^2 \quad (51)$$

Similarly the variation of the response surface \hat{S} from \bar{S} is denoted as SS_r , so that

$$SS_r = \sum_{j=1}^n (\hat{S}_j - \bar{S})^2 \quad (52)$$

SS_S and SS_r are called *total sum of squares* and *regression sum of squares*, respectively. The *coefficient of multiple determination*, denoted as R^2 , measures the fraction of the variation in the data

$$R^2 = \frac{SS_r}{SS_S} \quad (53)$$

The value of R^2 is between zero and one usually indicating a better fit for higher values. If more regressors are added to the model the value of R^2 will increase. However, this does not necessary mean that the prediction capabilities of the model improve. For this reason, there is an adjusted form of R^2 that is used to compare the different models and is given by

$$R_a^2 = 1 - \frac{(n-1)}{(n-n_S)} (1 - R^2) \quad (54)$$

for which the value also is between zero and one indicating a better fit for higher values. An additional test of a response surface is to evaluate it in a set of well-chosen test points not used in the regression procedure.

4.7 Comparison between different models

In the second order polynomial, here referred to as Model 2, no terms are eliminated so all the 10 terms is included

$$\begin{aligned} {}^2PI_{\text{avg}} = & 32.8 - 0.886 \cdot d_1 - 8.80 \cdot d_2 - 12.1 \cdot d_3 - \\ & 3.42 \cdot d_1^2 - 1.74 \cdot d_1 d_2 + 83.1 \cdot d_1 d_3 + 7.31 \cdot d_2^2 + \\ & 11.2 \cdot d_2 d_3 + 9.62 \cdot d_3^2 \end{aligned} \quad (55)$$

Both forward and backward elimination worsen the fit of the third order polynomial, here referred to as *Model 3*, thus all the 20 terms are included in the response surface

$$\begin{aligned} {}^3PI_{\text{avg}} = & 27.8 + 13.5 \cdot d_1 - 4.70 \cdot d_2 + 1.25 \cdot d_3 - \\ & 24.0 \cdot d_1^2 - 24.0 \cdot d_1 d_2 + 166 \cdot d_1 d_3 + 17.4 \cdot d_2^2 + \\ & 14.0 \cdot d_2 d_3 + 17.9 \cdot d_3^2 + 10.5 \cdot d_1^3 + 4.80 \cdot d_1^2 d_2 - \\ & 38.8 \cdot d_1^2 d_3 + 17.9 \cdot d_1 d_2^2 - 37.1 \cdot d_1 d_2 d_3 - 425 \cdot d_1 d_3^2 - \\ & 11.8 \cdot d_2^3 - 6.08 \cdot d_2^2 d_3 - 20.1 \cdot d_2 d_3^2 - 16.5 \cdot d_3^3 \end{aligned} \quad (56)$$

Forward elimination gives the best fit of the fourth order polynomial, here referred to as *Model 4-f*. Four terms are eliminated and leave the response surface with 31 terms

$$\begin{aligned} {}^4PI_{\text{avg}} = & 21.8 + 43.8 \cdot d_1 + 5.24 \cdot d_2 + 42.8 \cdot d_3 - \\ & 91.9 \cdot d_1^2 - 86.7 \cdot d_1 d_2 + 124 \cdot d_1 d_3 - 0.753 \cdot d_2^2 - \\ & 15.7 \cdot d_2 d_3 - 59.7 \cdot d_3^2 + 71.4 \cdot d_1^3 + 30.2 \cdot d_1^2 d_2 + \\ & 143 \cdot d_1^2 d_3 + 147 \cdot d_1 d_2^2 + 205 \cdot d_1 d_2 d_3 - 884 \cdot d_1 d_3^2 - \\ & 14.6 \cdot d_2^3 + 38.1 \cdot d_2^2 d_3 - 29.5 \cdot d_2 d_3^2 + 25.3 \cdot d_3^3 - \\ & 23.2 \cdot d_1^4 - 14.6 \cdot d_1^2 d_2^2 - 109 \cdot d_1^2 d_2 d_3 - 773 \cdot d_1^2 d_3^2 - \\ & 73.9 \cdot d_1 d_2^3 - 249 \cdot d_1 d_2^2 d_3 + 193 \cdot d_1 d_2 d_3^2 + 813 \cdot d_1 d_3^3 + \\ & 13.3 \cdot d_2^4 - 22.4 \cdot d_2^3 d_3 + 36.7 \cdot d_2 d_3^3 \end{aligned} \quad (57)$$

The fifth order reduced polynomial, here referred to as *Model 5-b*, obtained by backward elimination, is the best of the four models and the elimination removes nine

Model	R_a^2	σ_a/\bar{S} x100	\bar{S}	σ_t/\bar{S} x100	\bar{S}_t
2	0.78	3.61%	31.27	4.18%	31.34
3	0.90	2.44%	31.27	2.43%	31.34
4-f	0.97	1.25%	31.27	1.92%	31.34
5-b	0.99	0.79%	31.27	1.38%	31.34

Table 2 : Accuracy data generated with *JMP* and for the 42 test points.

terms. The resulting response surface with 47 terms is given by

$$\begin{aligned}
{}^5P_{I_{avg}} = & 14.4 + 85.7 \cdot d_1 - 14.4 \cdot d_2 + 142 \cdot d_3 - \\
& 168 \cdot d_1^2 - 63.1 \cdot d_1 d_2 - 193 \cdot d_1 d_3 + 7.74 \cdot d_2^2 + \\
& 51.3 \cdot d_2 d_3 - 472 \cdot d_3^2 + 107 \cdot d_1^3 + 24.5 \cdot d_1^2 d_2 + \\
& 473 \cdot d_1^2 d_3 + 168 \cdot d_1 d_2^2 + 892 \cdot d_1 d_2 d_3 - 781 \cdot d_1 d_3^2 + \\
& 47.3 \cdot d_2^3 - 43.4 \cdot d_2^2 d_3 - 121 \cdot d_2 d_3^2 + 716 \cdot d_3^3 - \\
& 17.5 \cdot d_1^4 - 26.4 \cdot d_1^3 d_2 + 372 \cdot d_1^3 d_3 + 128 \cdot d_1^2 d_2^2 - \\
& 1489 \cdot d_1^2 d_2 d_3 - 1515 \cdot d_1^2 d_3^2 - 303 \cdot d_1 d_2^3 - \\
& 905 \cdot d_1 d_2^2 d_3 - 1658 \cdot d_1 d_2 d_3^2 + 3422 \cdot d_1 d_3^3 - \\
& 32.0 \cdot d_2^4 - 176 \cdot d_2^3 d_3 + 318 \cdot d_2^2 d_3^2 + 85.9 \cdot d_2 d_3^3 - \\
& 502 \cdot d_3^4 - 409 \cdot d_1^4 d_3 - 27.4 \cdot d_1^3 d_2^2 + 699 \cdot d_1^3 d_2 d_3 - \\
& 44.9 \cdot d_1^2 d_2^3 + 3151 \cdot d_1^2 d_2 d_3^2 + 142 \cdot d_1 d_2^4 + \\
& 598 \cdot d_1 d_2^3 d_3 + 1261 \cdot d_1 d_2 d_3^3 - 2961 \cdot d_1 d_3^4 + \\
& 95.3 \cdot d_2^4 d_3 - 242 \cdot d_2^3 d_3^2 + 132 \cdot d_2^5 \quad (58)
\end{aligned}$$

In addition to the 250 points that the response surfaces are based on, 42 points were generated, which are used as test points. The accuracy increases with increased order of the polynomial response surface. That can also be seen in Table 2 showing the accuracy statistics of the four models. The data is generated with *JMP* except for the two right most columns showing the relative error and the mean of the test points.

4.8 Optimization of the response surface

Model 5-b consisting of the reduced fifth order polynomial, Eq. (58), is used for optimization over the normalized design space d_1 , d_2 and d_3 , Eqs. (48), in order to maximize the average power index. *Solver*, an optimization tool available as part of *Microsoft Excel* [Microsoft Corporation (1985 – 1996)] package, is used in this effort. This tool uses the *Generalized Reduced Gradient (GRG2)* nonlinear optimization code developed by Ladsen, Waren, Jain and Ratner (1978). The average power index is maximized with the constraints on power, prestress, and elastic modulus

$$\begin{aligned}
0.3 \leq z \leq 7 \\
1.0\text{N/m}^2 \leq {}^0S \leq 80\text{kN/m}^2 \\
E \geq 1.7\text{MN/m}^2 + 1/z \cdot 5.5\text{MN/m}^2 \\
E \leq 0.84\text{MN/m}^2 + 1/z \cdot 2.4\text{MN/m}^2 \quad (59)
\end{aligned}$$

The constraints for the elastic modulus are dependent on z . The constraint functions, Eqs. (59), are generated with regression analysis in *Excel* using the constraints for the different z -values. The maximum point within the constraints is ${}^0S_{ref}=1.0\text{N/m}^2$, $z=4.95$ and $E=2.8\text{MN/m}^2$ which agrees well with XFOIL. Four other local maximum values were found.

The dashed lines in Fig. 8 show the instantaneous membrane shapes produced by XFOIL with the optimized membrane properties in comparison with the solid line, which is the rigid shape. The freestream Reynolds number was fluctuating 30% about its mean value 8.0×10^4 and at an angle of attack 3° . As discussed before the semi-flexible airfoil and the rigid airfoil should have approximately the same initial thickness in order to be able to do meaningful comparisons between the two airfoils. The upper dashed lines correspond to the membrane shapes for higher Reynolds numbers and vice versa. It is clear that the thickness of the semi-flexible airfoil increases when the freestream increases and decreases when the freestream decreases. Furthermore, we note that the highest point of the membrane moves somewhat forward at reduced Reynolds number.

Figure 9 shows from upper left the lift coefficient, the C_l/C_d ratio, the power index and the normalized y-coordinate position of node 47. The semi-flexible airfoil

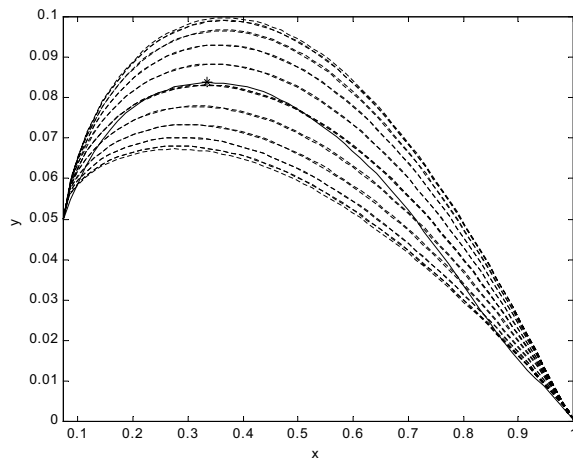


Figure 8 : Membrane shapes (dashed lines) produced by XFOIL for the optimum design $^0S_{ref}=1.0N/m^2$, $z=4.95$ and $E=2.8MN/m^2$ compared with the rigid shape (solid line) at $\alpha = 3^\circ$ in a 30% fluctuating flow around the mean Reynolds number value 8.0×10^4 .

experiences a much better lift coefficient in both the high Reynolds number region and the low Reynolds number region. For lower Reynolds numbers the rigid airfoil’s lift coefficient breaks down because of a massive separation. Both the C_l/C_d ratio and the power index are better for the semi-flexible airfoil in the whole unsteady cycle. The advantage is most pronounced at the top and bottom values of the Reynolds number.

Figure 10 shows from upper left the lift coefficient, the C_l/C_d ratio, the power index, the normalized y -coordinate position of the membrane at a representative location, the angle of attack and the lift for the comparison in the constant lift formulation described in Eqs. (24)-(28). This exercise is done to illustrate the effect of angle of attack adjustment during unsteady flight. Each cycle is discretized in 100 time steps and the normalized amplitude of the freestream fluctuation is 0.15. Three time periods are used, namely 0.5, 1.5 and 3 seconds. Both and semi-flexible airfoils seem to have approximately the same lift and lift coefficient throughout the cycle but the semi-flexible airfoil exhibits a larger variation in angle of attack. But similar to the simulations with constant angle of attack, both the C_l/C_d ratio and the power index are better for the semi-flexible airfoil in the whole unsteady cycle. The variation in lift seems to decrease with increased time period as expected for both the airfoils while the variation in angle of attack increases.

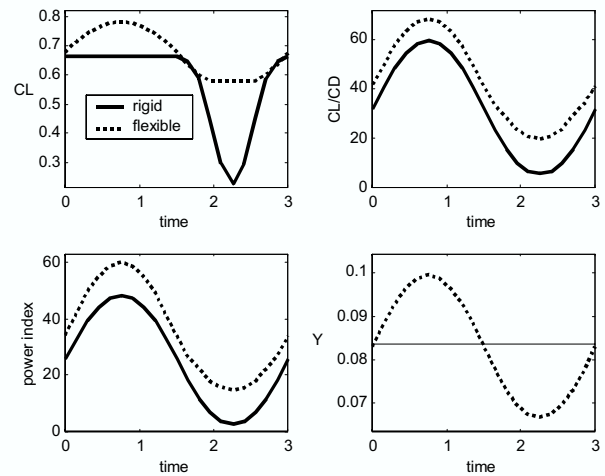


Figure 9 : Comparison between semi-flexible and rigid results produced by XFOIL for the optimum design $^0S_{ref}=1.0N/m^2$, $z=4.95$ and $E=2.8MN/m^2$ at $\alpha = 3^\circ$ in a 30% fluctuating flow around the mean Reynolds number value 8.0×10^4 .

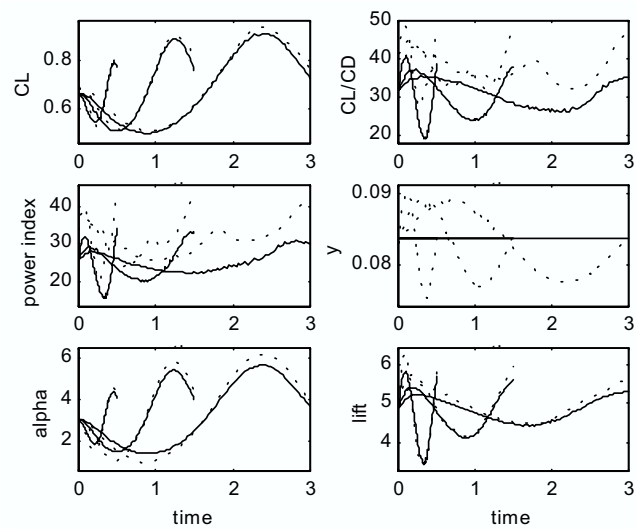


Figure 10 : Comparison between semi-flexible (dashed lines) and rigid (solid lines) predictions for the optimum design when the angle of attack is let to vary according to the constant lift formulation in a 15% fluctuating amplitude of the freestream.

5 Conclusions

The flexible airfoil considered is for a membrane attached on the upper surface of a modified Clark-Y airfoil. The membrane is free to move upwards and downwards according to the pressure difference across it. 250 computational simulations were done with a modified version of XFOIL in a 30% fluctuating freestream about the mean Reynolds number 8.0×10^4 at 3 degrees of angle of attack. The membrane prestress, elastic modulus and thickness distribution were varied. It is found that the maximum membrane y -value moves backward towards the center of the airfoil for increasing prestress and the membrane deflection increases with decreased elastic modulus. Response surfaces were created for the average power index by standard least square regression analysis using the normalized design variables. A reduced fifth order polynomial showed the best agreement to the set of points used for regression and 42 test points, different from those used for the fit. The maximum response found by *Excel* was for (i) low prestress, (ii) thickness varying with $s^{4.95}$, and (iii) an elastic modulus of 2.8 MN/m^2 . The average power index in the whole unsteady cycle for the semi-flexible airfoil was 35.9 while the rigid airfoil only received a value of 25.6. The rigid airfoil exhibited a severe dip in lift coefficient at the lower Reynolds number region, while the semi-flexible airfoil did not show any such tendency. The present study has not only confirmed the usefulness of flexible airfoils in an unsteady low Reynolds number environment, but also established a framework of optimizing the interplay among the key design parameters of the membrane. While the quantitative details will obviously change with the selection of different airfoil shapes, the qualitative trends established in the present study will be useful for developing technologies in the area of low Reynolds number aerodynamics.

Acknowledgement: The present work has been supported by AFOSR.

References

- Drela, M.** (1989): XFOIL: An Analysis and Design System for Low Reynolds Number Airfoils. *Low Reynolds Number Aerodynamics*, Springer-Verlag, New York, pp. 1-12.
- Drela, M.** and **Giles, M. B.** (1987): Viscous-Inviscid Analysis of Transonic and Low Reynolds Number Airfoils. *AIAA Journal*, Vol. 25, pp. 1347-1355.
- Ladson, L.S., Waren, A., Jain, A. and Ratner, M.** (1978): Design and Testing of a Generalized Reduced Gradient Code for Nonlinear Programming. *ACM Transactions on Mathematical Software*, 4:1 (1978).
- Microsoft Corporation (1985 – 1996): *Microsoft Excel 97*.
- Myers, R. H. and Montgomery, D. C.** (1995): Response Surface Methodology – Process and Product Optimization Using Designed Experiment. *John Wiley & Sons*.
- Okumura, H. and Kawahara, M.** (2000): Shape Optimization of Body Located in Incompressible Navier-Stokes Flow Based on Optimal Control Theory, *CMES: Computer Modeling in Engineering & Sciences*, Vol. 1, pp. 71-78.
- Rugonyi, S. and Bathe, K.J.** (2001): On Finite Element Analysis of Fluid Flows Fully Coupled with Structural Interactions, *CMES: Computer Modeling in Engineering & Sciences*, Vol. 2, pp. 195-212.
- SAS Institute Inc. (1995): *JMP version 3*. Cary, NC.
- Shyy, W., Berg, M. and Ljunqvist, D.** (1999): Flapping and Flexible Wings for Biological and Micro Air Vehicles. *Progress in Aerospace Sciences*, Vol. 35, No 5, pp. 455-506.
- Shyy, W., Jenkins, D. A. and Smith, R. W.** (1997): Study of Adaptive Shape Airfoils at Low Reynolds Number in Oscillatory Flows. *AIAA Journal*, Vol. 35, No. 9, pp. 1545-1548.
- Shyy, W., Klevebring, F., Nilsson, M., Sloan, J., Carroll, B. and Fuentes, C.** (1999): Rigid and Flexible Low Reynolds Number Airfoils. *Journal of Aircraft*, Vol. 36, No. 3, pp. 523-529.
- Shyy, W., Papila, N., Vaidyanathan, R. and Tucker, P.K.** (2001): Global Design Optimization for Aerodynamics and Rocket Propulsion Components, *Progress in Aerospace Sciences*, Vol. 37, pp.59-118.
- Shyy, W. and Smith, R.** (1997): A Study of Flexible Airfoil Aerodynamics with Application to Micro Aerial Vehicles. *AIAA-97-1933*.
- Shyy, W., Udaykumar, H. S., Rao, M. M., and Smith, R. W.** (1996): Computational Fluid Dynamics with Moving Boundaries. Taylor & Francis, Washington, D.C..